ABOUT THE CORRECTED PHASE TRANSFORMATION ZONES OF SHAPE MEMORY ALLOYS' FRACTURE TESTS ON SINGLE EDGE-CRACKED SPECIMEN

V. TAILLEBOT, C. LEXCELLENT
Département Mécanique Appliquée, Institut FEMTO-ST, 25000 Besançon, France

P. VACHER
Laboratoire SYMME, Polytech'Savoie, 74944 Annecy le Vieux, France

The thermomechanical behavior of shape memory alloys is now well mastered. However, a hindrance to their sustainable use is the lack of knowledge of their fracture behavior. With the aim of filling this partial gap, fracture tests on edge-cracked specimens in NiTi have been made. Particular attention was paid to determine the phase transformation zones in the vicinity of the crack tip. In one hand, experimental kinematic fields are observed using digital image correlation showing strain localization around the crack tip. In the other hand, an analytical prediction, based on a modified equivalent stress criterion and taking into account the asymmetric behavior of shape memory alloys in tension-compression, provides shape and size of transformation outset zones. Experimental results are relatively in agreement with our analytical modeling.

Keywords : Shape memory alloys – phase transformation – fracture – NiTi - DIC

Shape Memory Alloys (SMA) are widely used in smart structures: actuators, medical devices and aeronautical materials. A particular reason for this is its very large recoverable strains (of the order of 8% for equiatomic NiTi) associated with their pseudoelastic behaviour. The extended use of SMA, sometimes subjected to rather complex loadings, raises the issue of the service life of systems and leads us to investigate the SMA fracture and/or fatigue damage.

Pseudoelasticity is associated with a martensitic Phase Transformation (PT), induced by an applied load, between high-symmetry austenite and low-symmetry martensite. Martensitic PT occurring in the vicinity of crack tip plays an important role on the stress distribution around the crack tip. A lot of studies have been carried out to investigate the fatigue behavior of SMA especially on nitinol (see Refs. 1 and 2 for more details).

We can cite an experimental work from Ref. 3 about the fatigue-crack growth and the fracture toughening behaviour of a tube. They show a higher fatigue threshold and a lower measured toughness than previously report values for bulk NiTi material.(S.W. In Ref. 4), Robertson and R.O. Ritchie measured in-situ three dimensional strains, phases and crystallographic alignment ahead of a growing fatigue crack (100 cycles). Their measurements reveal that the majority of austenite grains were only subjected to only 0.5%-1.0% elastic strain despite a macroscopic pseudoelastic strain recovery of 6%-8% associated to the martensitic PT.

Although, recent numerical and FEM studies of fracture in SMA have been published (see Refs. 5 and 6), there is a lack of experimental observations of the phase transformation zones around the crack tip during fracture tests.

Coupled to a FEM computation, Daly et al., in Ref. 7, performed a tensile test on an edge-crack specimen of austenitic NiTi with an in-situ optical technique to examine the shape and the size of phase transformation zones. They measured at room temperature the fracture toughness K_{IC} for fine grained polycrystalline nitinol sheets.

More recently, Gollerthan et al., in Ref. 8, have examined the formation of the stress-induced martensite and its back-transformation to austenite on loading and unloading in front of crack tip of NiTi miniature CT specimen using IR thermography. They show that crack growth occurs into a stress-induced martensite microstructure, which immediately retransforms to austenite as the crack propagates past.

On an edged cracked specimen, the martensitic P.T. increases the yield toughening around the crack tip as it is the role of plasticity for any ductile classical material (see Refs. 5 and 7). An experimental investigation has been set up to observe strain localization during crack propagation on NiTi thin sheets (under Mode I loading).

Experimental P.T. onset zones are observed and compared to analytical predictions.

The material is a Ni-55.41-Ti 44.59 wt%, fully austenitic at room temperature. Tensile tests performed at 293 K, under a strain rate $\dot{\varepsilon} = 10^{-4} s^{-1}$ exhibit a pseudoelastic behavior with a wide associated hysteresis.

The yield stress σ_c associated with the martensitic P.T. outset is around 460 MPa. Strains associated to outset (austenite to martensite) and completion (fully martensite) are respectively 0.66% and 5.50%.

The dimension of the edge-cracked specimen are in agreement with the Handbook prescriptions (from Ref.9) for the stress intensity factor calculation: length: L = 50 mm, width: W = 30 mm, thickness: e = 2 mm, edge-crack length a = 10 mm). Several curvature radii ρ at the crack tip are tested and machined by spark-machining .

Fracture tests are made at the SYMME Laboratory, in Annecy le Vieux, on an INSTRON tensile machine, at room temperature at the displacement rate of $2.10^{-2} m.s^{-1}$.

Using the in situ optical technique of Digital Image Correlation (DIC), a pattern was applied on a specimen face prior to testing by first coating the sample in black paint and then finely speckling of white paint. Images were recorded using a 1280 x 1024 pixel (ie about 12.5 x 15.6 mm) CCD camera at 1 Hz.

The stress intensity factor K_I is obtained thanks to an empirical formulae (see Ref. 9) for $a/W \leq 0.6$

$$K_I = \sigma_o \sqrt{\pi a}\ f\left(\frac{a}{W}\right) \qquad (1)$$

with

$$f\left(\frac{a}{W}\right) = 1.122 - 0.231\left(\frac{a}{W}\right) + 10.55\left(\frac{a}{W}\right)^2 - 21.72\left(\frac{a}{W}\right)^3 + 30.39\left(\frac{a}{W}\right)^4 \qquad (2)$$

with $\sigma_o = \frac{F_o}{We}$, where F_o is the applied load.

Then, the ultimate strength measured (just before the specimen fracture) is used to compute K_{IC} the critical stress intensity factor (see table 1).

ρ (mm)	0.25	0.5	1	1.5
$K_{IC}\ (MPa\sqrt{m})$	91	102	108	115

Table 1- Critical stress intensity factor vs. curvature radius.

One has to note that the parameter K_{IC}, which corresponds to the sample the fracture toughness, increases with the curvature radius at the crack tip, thus reducing stress triaxiality degree. It means that K_{IC} does not constitute an intrinsic parameter of material fracture. Tests at room temperature performed from Ref. 7. have shown that K_{IC} is independent of the ratio a/W. They obtained $K_{IC} = 51.4$ MPa $\sqrt{m}$ for thin sheets of 30 x 13 x 0,16 mm^3. But this experimental investigation shows K_{IC} depends on the curvature radius of the crack tip.

Strain on the specimen surface is measured by DIC technique. Recorded images during fracture are post-processed with the software 7D developed by P.Vacher. It provides 2D-strain fields around the crack tip.
As in Ref. 7, the Green-Lagrange strain field ε_{yy} (where y is the direction normal to the crack tip) has been chosen as an indicator of the martensitic phase level in reference to the yield values obtained for the P.T. outset and end during previous tensile tests.

Figures 1,2,3 show a kidney shaped strain field ε_{yy} around the crack tip for ρ = 1 mm and for different applied loads: K_1 = 69 MPa $\sqrt{m}$ (Fig.1), K_I = 88 MPa $\sqrt{m}$ (Fig.2) and K_I = 108 MPa $\sqrt{m}$ (Fig.3). The two inclined lobes stretch progressively around the crack tip as the load increases.

A comparison between the observed phase transformation surfaces and the predicted ones is performed.

Thanks to the setting of an equivalent stress, an analytical yield surface of phase transformation outset is predicted by Lexcellent et al, see Ref. 10 for more details. Within the framework of the linear elastic fracture mechanics, asymmetric SMA behavior in tension-compression is integrated.
The yield surface of phase transformation outset is

$$F(\sigma) = \bar{\sigma}\, g(y_\sigma) - \sigma_c = 0 \qquad (3)$$

where

$$\sigma_c = b(T - M_S^o) \ , \ \bar{\sigma} = \left(\frac{3}{2} dev\underline{\sigma} : dev\underline{\sigma} \right)^{1/2} \ ,$$

$$y_\sigma = \frac{27 \det(dev\underline{\sigma})}{2\bar{\sigma}^3}$$

and $g(y_\sigma)$ is chosen as linear in y_σ i.e.

$$g(y_\sigma) = 1 + b y_\sigma \qquad (4)$$

The convexity of the surface F(σ) requires $0 \le b \le 1/8$. The case b = 0 corresponds to Huber Von Mises case where the asymmetry between tension and compression is not taken in account.

Moreover, in this present paper, analytical of outset P.T. zones results from a new formulation, soon published, that integrates the curvature radius.

According to plane stress conditions and mode I loading, two cases are presented with b = 0 on Fig.4 and b = 1/8 (maximum of asymmetry) on Fig.5. It shows that the asymmetry effect is not negligible on the size and especially on shape of the surfaces.

Firstly, for a fixed crack radius, the asymmetry parameter generates a fold over of the pseudo-cardioid (Fig.5). The areas computation shows that it also leads to an increase in transformation zone size.

Dealing with the loading case $K_I = 69MPa\sqrt{m}$, we compare the height of the outset transformation zones obtained through indirect strain measurements and computation based on equivalent stress. The analytical modeling (Fig.6) gives 11.3 mm. On Fig.7, a filter eliminates the deformation field for values $\varepsilon_{yy} \le 0.66\%$, where the P.T. has not yet started. Therefore, the average height is approximately estimated at 4,3 mm. The discrepancy could be explained by the great sensitivity of the parameter σ_c that is identified experimentally.

As a conclusion, this investigation on SMA fracture comprises two parts. Based on the knowledge of linear elastic fields, an analytical prediction gives the martensitic P.T. surfaces. The second aspect of this study is an experimental investigation with the aim of observing these transformation surfaces and correlating with theoretical predictions.

The complexity lies in the small-scale of the observable phenomenon which, greatly limits the accuracy of the size of transformation zones.

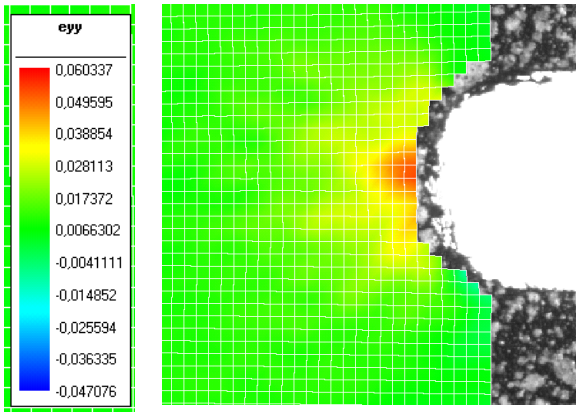

FIG.1 – Strain field ε_{yy} for applied $K_I = 69MPa\sqrt{m}$

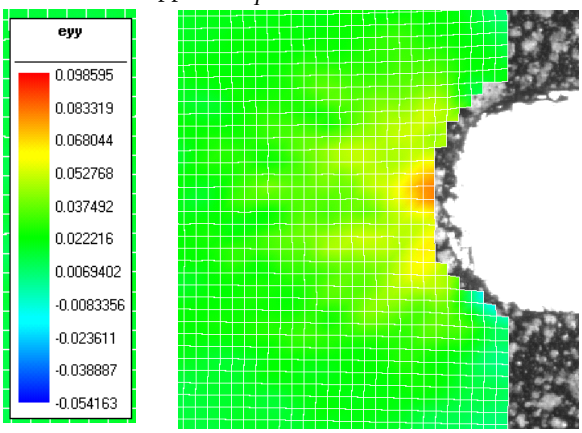

FIG.2 – Strain field ε_{yy} for applied $K_I = 88MPa\sqrt{m}$

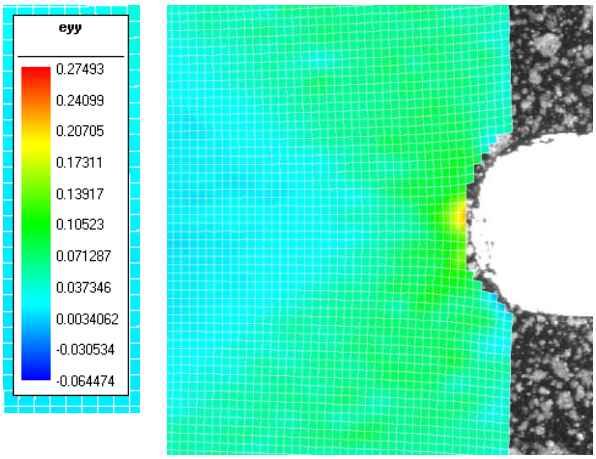

FIG.3 – Strain field ε_{yy} at fracture for applied $K_I = 108MPa\sqrt{m}$

Nevertheless, the experimental investigation agrees qualitatively with the theoretical modeling. Other experimental results and the analytical formulation of the P.T. surfaces including the curvature radius will be published soon.

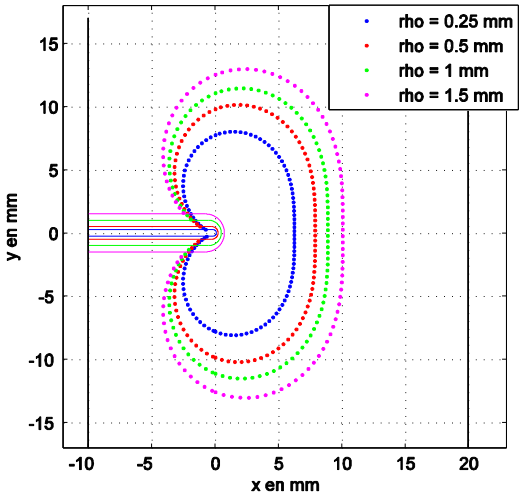

FIG.4 – Transformation outset surface for b = 0 (no asymmetry taken into account)

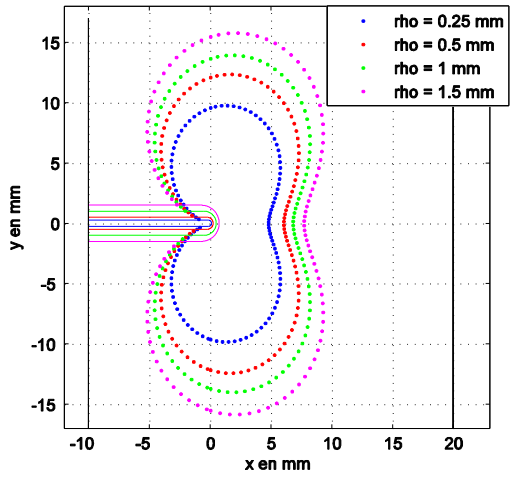

FIG.5 – Transformation outset surface for b = 1/8 (maximal asymmetry)

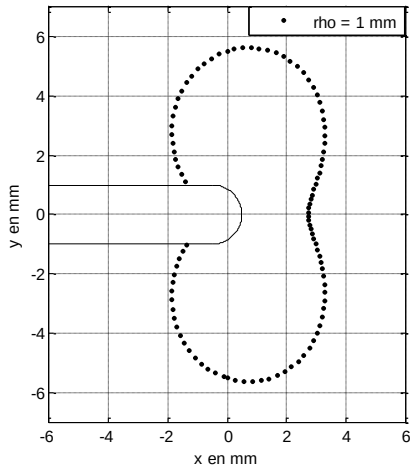

FIG.6 – Transformation outset surface computed for an applied $K_I = 69MPa\sqrt{m}$

In the future, local temperature measurements with its integration in the heat equation will reinforce our analysis.

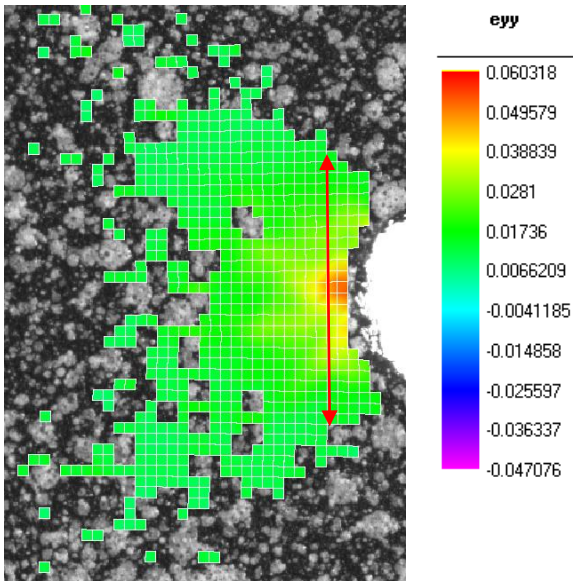

FIG.7 – Strain field ε_{yy} for applied $K_I = 69MPa\sqrt{m}$ showing $\varepsilon_{yy} > 0.66\%$.

References

1. A. McKelvey, R.O. Ritchie, Metallurgical and Material Transactions A, 32A 731 (2001).
2. A. Pelton, T. Duerig, D. Steckel, Minimally Invasive Therapy Allied Technologies, 13 218 (2004).
3. S.W. Robertson, R.O. Ritchie, Biomaterials, 28(4) 700 (2007).
4. S.W. Robertson, A. Mehta, A.R. Pelton, R.O. Ritchie, Acta Materiala, 55(18) 6198 (2007).
5. X.M. Wang, Y.F. Wang, A. Baruj, G. Eggeler, Z.F. Yue, Material Sciences and Engineering: A, 394(1–2) 393 (2005).
6. S. Yi, S. Gao, International Journal of Solids and Structures, 37(38) 5315 (2000).
7. S. Daly, A. Miller, G. Ravichandran, K. Bhattacharya, Acta Materiala, 55 6322 (2007).
8. S. Gollerthan, M.L. Young, K. Neuking, U. Ramamurty, G. Eggeler, Acta Materiala, 57 5892 (2009).
9. Y. Murakami, Stress intensity factors Handbook, 1st edition. Pergamon Press, Volume 1 (The Society of Materials Science, Japan, 1987), pp. 188.
10. C. Lexcellent, M.R. Laydi, V. Taillebot, International Journal of Fracture, 169 1 (2011).